Eur. Phys. J. A **30**, 263–274 (2006)
DOI 10.1140/epja/i2006-10122-9

THE EUROPEAN PHYSICAL JOURNAL A

Bimodalities: A survey of experimental data and models

O. Lopez[1,a] and M.F. Rivet[2]

[1] Laboratoire de Physique Corpusculaire, IN2P3-CNRS/ENSICAEN/Université, F-14050 Caen cedex, France
[2] Institut de Physique Nucléaire, IN2P3-CNRS, F-91406 Orsay cedex, France

Received: 13 February 2006 /
Published online: 25 October 2006 –

Abstract. Bimodal distributions of some chosen variables measured in nuclear collisions were recently proposed as a non-ambiguous signature of a first-order phase transition in nuclei. This section presents a compilation of both theoretical and experimental studies on bimodalities performed so far, in relation with the liquid-gas phase transition in nuclear matter.

PACS. 25.70.Pq Multifragment emission and correlations – 24.60.-k Statistical theory and fluctuations – 64.60.Cn Order-disorder transformations; statistical mechanics of model systems – 25.70.-z Low and intermediate energy heavy-ion reactions

After a formulation of the theoretical bases of bimodality, world-wide experimental results will be reviewed and discussed, as well as the occurrence of some kind of bimodality in models. Finally, conclusions on the perspectives of such analyses in the near future and the possible connections to other proposed signals of the liquid-gas phase transition in nuclear matter will be given.

1 Theoretical bases

1.1 Definition

Bimodality is a property of finite systems undergoing a first-order phase transition [1–3]. It is thus a generic feature which concerns not only nuclear physics but a broad domain of physics such as astrophysics, or soft-matter physics. Bimodality means that *the probability distribution of an order parameter of the considered system at phase transition exhibits two peaks separated by a minimum*. Indeed, if the system is in a pure phase, the order parameter distribution consists in one peak and can be characterized by its mean value and its variance. By contrast, if the system is in the coexistence region, the distribution presents two peaks, well separated, whose properties are related to the two different phases of the system [2]. Bimodality is then one of the signals associated to a first-order phase transition [3], beside others such as scaling laws, critical exponents or negative heat capacities.

In the following, the term "bimodality" will abbreviate "the probability distribution of some variable, in a given region of the phase diagram of the system, is bimodal".

[a] e-mail: lopezo@lpccaen.in2p3.fr

1.2 Pioneering studies

Bimodality and its relationship to phase transition has been studied since the '80s. Figure 1 shows an Ising model simulation of a ferromagnet studied by Binder and Landau [4]. In this analysis, the authors studied the magnetization M of the system as a function of the applied magnetic field H. When the magnetic field comes close to the critical value H_c, the spontaneous magnetization of the ferromagnet presents a sudden change; in this case the probability distribution of the magnetization is never bimodal, as the system "jumps" suddenly from the negative value $-M_{sp}$ to the positive one $+M_{sp}$: the transition between the two regimes is sharp at the thermodynamical limit.

By contrast, when the size of the system is finite (and defined by the number of sites L), the step function is replaced by a smooth curve in fig. 1, with a slope proportional to L^d —where d is the dimensionality of the system. Consequently, in the vicinity of H_c, the magnetization M exhibits a bimodal structure, as shown in the bottom panel of fig. 1.

1.3 Link with phase transition in thermodynamics

It was recently demonstrated by Chomaz and Gulminelli that bimodality of the probability distribution of the order parameter is equivalent to the other definitions of phase transition proposed up to now [5].

1.3.1 Relationship to the Yang-Lee theorem

The Yang-Lee theorem [6] is considered as the standard definition of first-order phase transitions at the thermo-

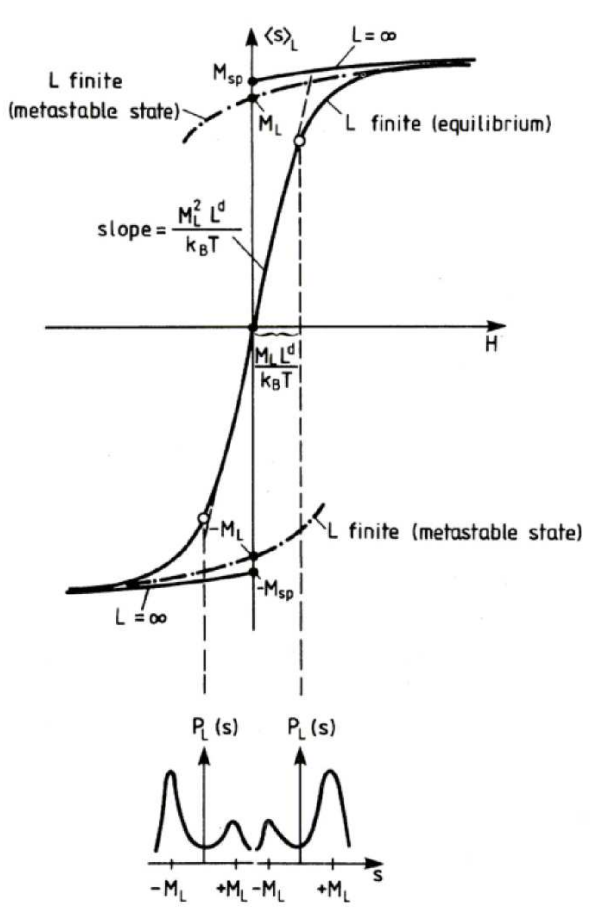

Fig. 1. Evolution of the magnetization M, as a function of the applied magnetic field H, in the Ising model for a lattice defined by the size L. The bottom panel presents a schematic probability distribution of the magnetization between $-M_L$ and $+M_L$ around the critical field value H_c. Taken from [4].

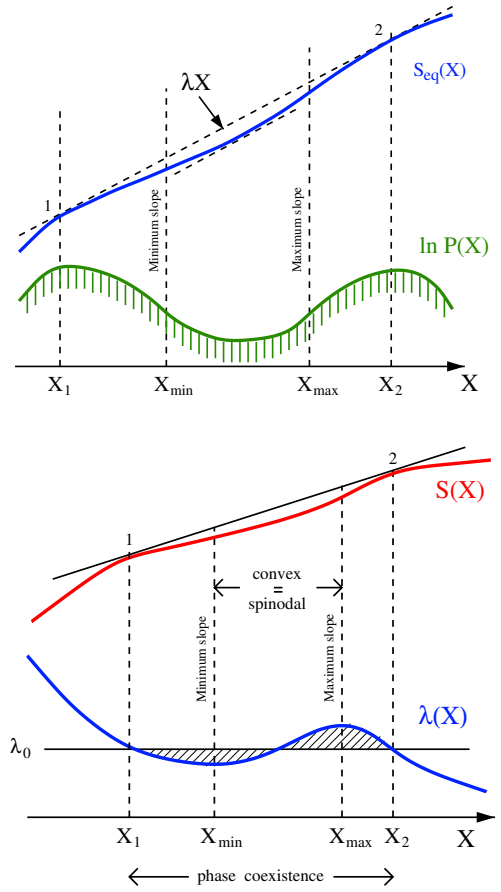

Fig. 2. Entropy S of the system as a function of an order parameter X of the phase transition. The relation is made between the convex intruder of S, the bimodal distribution in X (top) and the abnormal fluctuations of X in the phase coexistence region (bottom). λ is the intensive variable associated with X. Taken from [7].

dynamic limit. As demonstrated in [5], bimodality is a necessary and sufficient condition for zeroes of the partition sum in the control intensive variable complex plane to be distributed on a line perpendicular to the real axis.

1.3.2 Anomaly of thermodynamical potentials

A first-order phase transition is characterized by an *inverted curvature* of the relevant thermodynamical potential (entropy, free energy) [7,8]. This feature is also equivalent to a bimodality in the event probability of the given order parameter X as displayed in the upper part of fig. 2.

1.3.3 Negative derivatives of the thermodynamical potentials

A first-order phase transition was also related to a backbending in the equation of state of the system [7], characterized by a negative second derivative of the thermodynamical potential, as, for example, the heat capacity if the energy is the order parameter, fig. 2 bottom.

1.4 Microcanonical vs. canonical ensemble

Among the observables signing a phase transition, the heat capacity is related to the fluctuations of the partial energy of the system and needs to be studied in the microcanonical ensemble, while bimodality can only be observed when the system is free to fluctuate in terms of the associated extensive variable (*i.e.* energy or volume). This case corresponds to canonical or isobar ensembles. In other words, events must be selected without constraint on the extensive variable in order to study bimodality. However, in nuclear-physics experiments, the two colliding nuclei form an isolated system: it seems thus natural to work in a microcanonical ensemble, and cuts can be applied on the energy of the system, determined, for instance, by calorimetry. It seems conversely out of reach

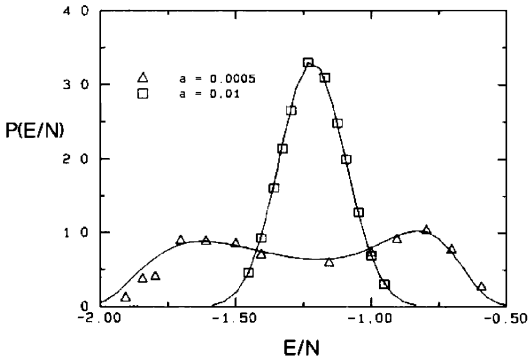

Fig. 3. Energy distributions obtained in the Gaussian ensemble for different $a = N/N'$. Taken from [9].

to be in a canonical framework which would require the existence of a large heat bath.

The situation is not hopeless, as it was shown some years ago that properties of phase transitions can be observed even if the working ensemble is not strictly microcanonical or canonical, but is an interpolating ensemble. In Gaussian ensembles, for instance, it is supposed that N particles are in contact with a system of N' particles acting as a heat bath at temperature T. When N' varies from 0 to ∞, the working ensemble mimicks the transition between microcanonical and canonical [9]. Figure 3 presents the results of such a simulation, where it is clearly seen that the probability distribution of the energy —in the transition region— presents a bimodal shape only when N/N' is small enough ($< 1/1000$), while for larger N/N', the situation is that of the microcanonical case with only one peak in the distribution.

1.5 Liquid-gas phase transition

Since nuclei are supposed to undergo a liquid-gas phase transition, specific studies of this peculiar transition were undertaken through lattice-gas calculations. In liquid-gas phase transitions, volume as well as energy are order parameters. The bimodality of the event probability distribution in the first-order phase transition region is evident in fig. 4 which shows the location of events in the volume *vs.* energy plane (top left). The projections along the axes (E, V) also display the expected bimodality, as does a linear combination of these two order parameters (bottom right). In this framework (lattice-gas model), bimodality is evidenced if we are able to select (sort) events in a canonical way (or as close as possible, see previous section), and plot the event probability distribution of the energy or volume, or any observable directly related to them.

2 Experimental observations

Since bimodality was proposed as a signature of liquid-gas phase transition, it was extensively searched for in event samples resulting from nuclear collisions; studies were

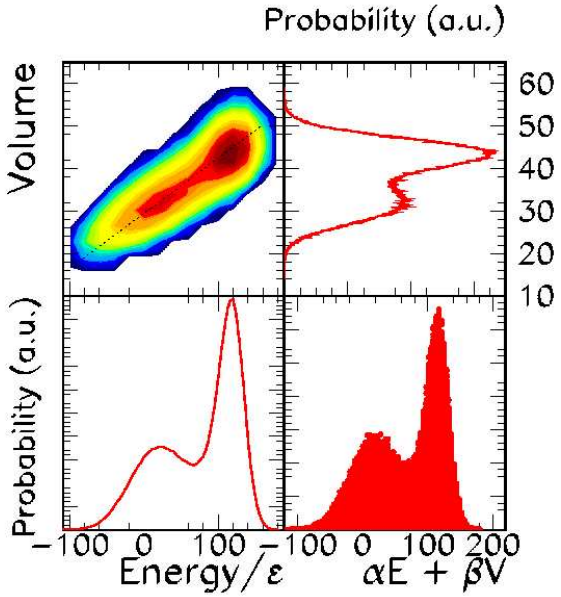

Fig. 4. Probability distributions of the energy E, volume V and a combination of the two variables coming from a lattice-gas simulation in the canonical ensemble. Taken from [2].

made for central collisions, where the liquid-gas phase transition is clearly evidenced by previous analyses (see sect. "Signals of phase transition", this topical issue) as well as for peripheral collisions, where a large range of excitation energy can be explored.

2.1 Central collisions: systems with mass $\sim$ 250

Systems with total mass close to 250 were studied with the INDRA array using two entrance channels, an asymmetric one, Ni + Au, and an almost symmetric one, Xe + Sn. In both cases, in the incident energy range scanned, it was shown that a fused system was formed in central collisions.

Bellaize *et al.* [10] have reported the observation of bimodality of the size asymmetry of the two largest fragments in central events for the Ni + Au system at 32 A, 52 A and 90 A MeV. It was associated with two fragmentation patterns (see first row of fig. 5), one similar to residue-evaporation (one large fragment with few small ones, zone 1 in fig. 5), the other to multifragmentation (fragments of nearly equal size, zone 2). A variable built with the charges of the three largest fragments, Z_1, Z_2, Z_3 in decreasing order,

$$Z_1 - 3(Z_2 + Z_3), \tag{1}$$

also has a bimodal distribution at 32 A and 52 A MeV, as shown in the bottom row of fig. 5, but no longer at 90 A MeV. This fact is compatible with the location of the system in the coexistence region below 52 A MeV, where it can experience a first-order phase transition by exploring different densities and temperatures. For higher energies (here 90 A MeV), the system passes directly through the

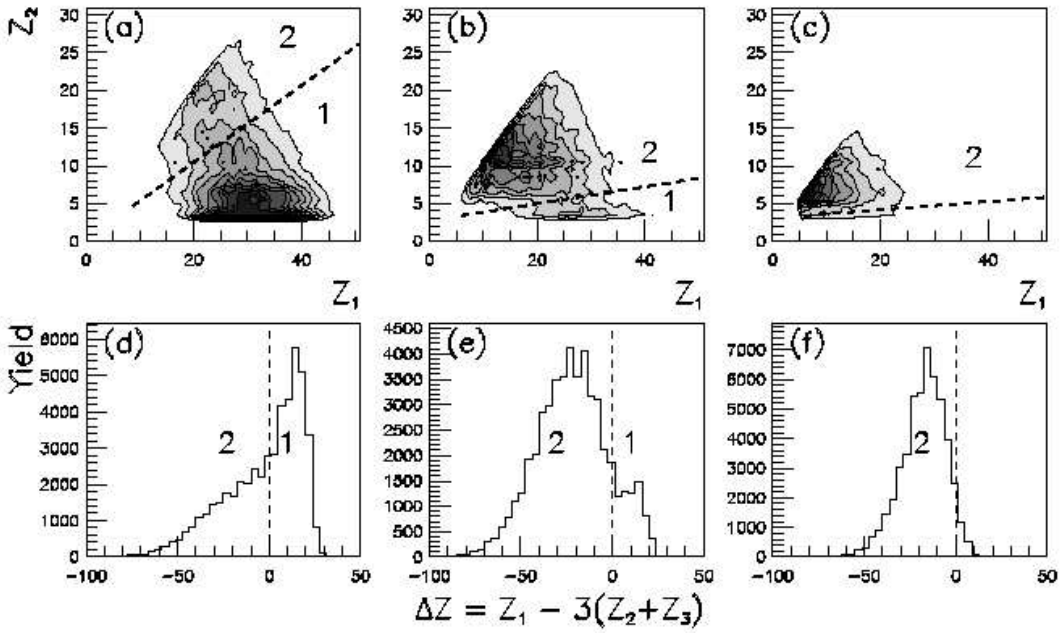

Fig. 5. Correlation between the two largest fragments, Z_1 and Z_2 obtained in central collisions for the Ni + Au system at 32 A (left), 52 A (middle) and 90 A MeV (right). The bottom row shows an asymmetry variable built as a linear combination of the atomic number of the three largest fragments. Taken from [10].

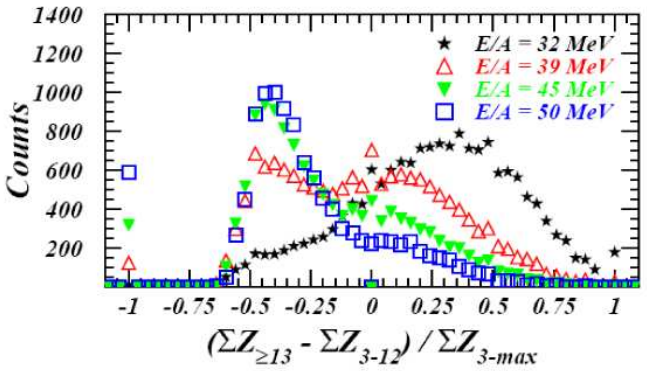

Fig. 6. Probability distributions of the charge asymmetry between light (Z = 3–12) and heavy fragments ($Z \geq 12$) for fused events in the Xe + Sn system at 32 A, 39 A, 45 A and 50 A MeV. Taken from [11].

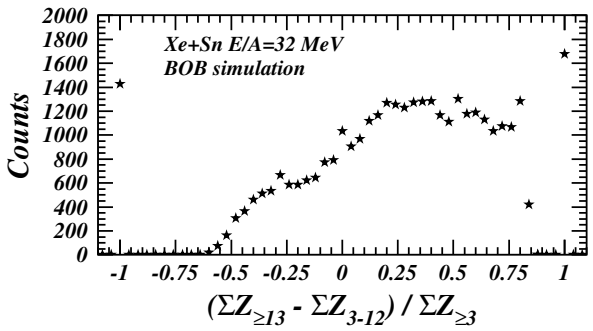

Fig. 7. Charge asymmetry obtained by using a stochastic mean-field simulation (BOB [12]) for central events of the Xe + Sn system at 32 A MeV. Unpublished results from the authors of [14].

coexistence region and we observe only the presence of the multifragmentation regime, which could indicate that the system explores only the low-density part of the phase diagram.

Figure 6 shows the distributions obtained when looking at the asymmetry ratio between heavy, ($Z \geq 13$), and light, (Z = 3–12), fragments

$$\left(\sum Z_{\geq 13} - \sum Z_{3-12}\right) / \sum Z_{\geq 3} \qquad (2)$$

for single-source events produced in central Xe + Sn collisions between 32 A and 50 A MeV [11]. Bimodality is present at all energies, with dominant "liquid-type" events at 32 A MeV, and a dominance of "gas-like" events at and above 45 A MeV; the two types of events are in roughly equal number at 39 A MeV, where other phase transition signals have been already observed (see contribution V.5, *Many-fragment correlations and possible signature of spinodal fragmentation*, this topical issue). The authors of [11] relate the chosen asymmetry variable to the density difference between the coexisting liquid and gas phases of nuclear matter. The same variable was built for the events resulting from a stochastic mean-field simulation [12] of head-on collisions between Xe and Sn at 32 A MeV. In this simulation, which was shown to well reproduce many experimental features, single variable distributions as well as different correlations [13–15] (see contribution V.5, *Many-fragment correlations and possible signature of spinodal fragmentation*, this topical issue), the system enters the co-

existence region and multifragments through spinodal decomposition. The equivalent of fig. 6 for simulated events is shown in fig. 7; the picture is very similar to the experimental data at the same energy (black stars in fig. 6), a bimodal behaviour appears with a dominance of events of liquid type.

2.2 Central collisions: systems with mass $\sim$ 100

Central collisions between two ^{58}Ni nuclei were studied at incident energies between 32 and 90 A MeV; event selection was made through a discriminant factorial analysis trained, at variance with ref. [16], on the complete experimental events. A bimodal distribution of the largest fragment was observed at 52 A MeV, intermediate between the Gaussian distributions measured at lower energies and the asymmetric distributions found from 74 A MeV upwards [17], see fig. 8. The minimum is rather shallow (about 80% of the peak value); at 64 A MeV a bimodal distribution persists, but now the peak on the more fragmented side is dominant. Conversely, the distributions of the fragments of higher rank (not shown) are monotonous. To our knowledge, this is the only direct observation of bimodality on the largest fragment.

2.2.1 Going further

Central collisions allowed to study and evidence a bimodal behaviour of some asymmetry variables, which can be connected to the density difference between a liquid and a gas phase; in that sense they would be good candidates for being order parameters of a liquid-gas–type transition. Nevertheless, several drawbacks can be pointed out; firstly it was shown that the lighter fragments exhibit a pre-equilibrium component in Ni + Au [10], while radial-flow effects were recognised in symmetric systems, Xe + Sn [18–20] and Ni + Ni [17]. But above all, the sorting of central events selects a rather narrow region in excitation energy for each incident energy (about 1–2 A MeV at half-maximum of the distribution). This is closer to a microcanonical working ensemble and may prevent a very clear observation of bimodality.

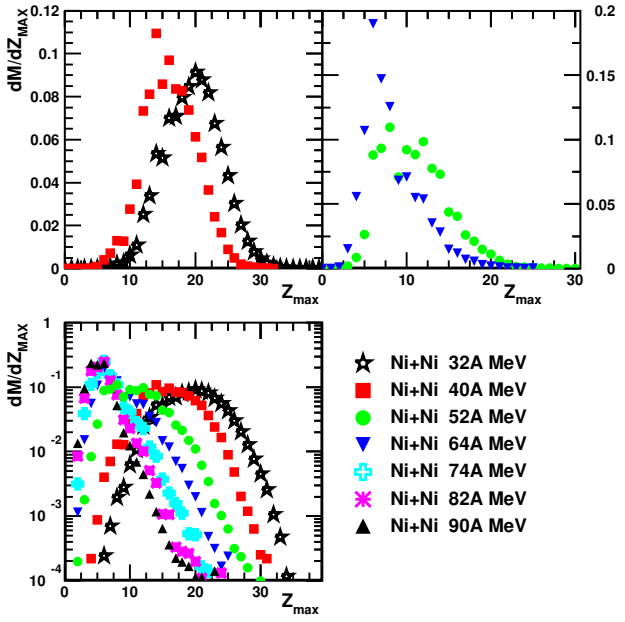

Fig. 8. Distributions of the largest fragment for central Ni + Ni collisions from 32 to 90 A MeV (bottom). The same distributions at the four lowest energies are displayed in linear scale in the top panels. Taken from [17].

2.3 Quasi-projectiles in peripheral collisions

Analyses of quasi-projectiles formed in peripheral and semi-peripheral reactions are thus mandatory, as they allow to overcome some of the abovementioned problems. In particular a broad excitation energy distribution of quasi-projectiles (QP) can be accessed. Exchanges of energy and particles with the quasi-target (QT), while it lies in the neighbourhood of the QP and especially when it is heavy, mimick a small heat bath and an almost canonical sorting can be envisaged. Whenever the incident energy is high enough, the different components (the QT and the QP, and the pre-equilibrium or neck part) can be better disentangled, or at least the uncertainties caused by their existence can be circumvented.

Most of the studies on quasi-projectiles arise from Au on Au collisions at various energies. Extensive results concerning a very light nucleus, close to argon were also recently proposed. Several variables are used for sorting events as a function of the violence of the collisions; among the most commonly employed one can cite multiplicities and the transverse energy (relative to the beam axis) of charged products, either all of them or only light charged

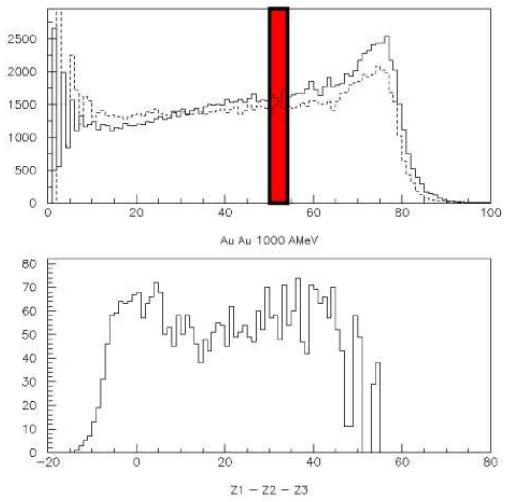

Fig. 9. Z_{bound} (top) and charge asymmetry distributions (bottom) for the Au + Au system at 1 A GeV. The bottom panel corresponds to the Z_{bound} selection displayed by the highlighted area in the top panel. Taken from [27].

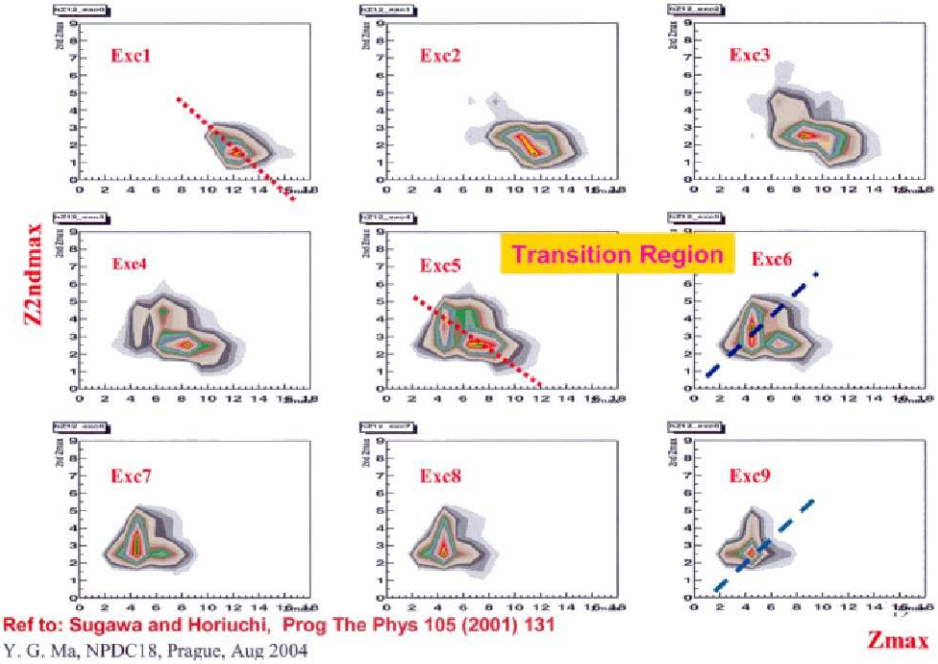

Fig. 10. Correlation between the largest charge (Z_{max}) and the second largest ($Z_{2nd\ max}$) for the QP in peripheral Ar + Ni collisions at 47 A MeV. Panels from Exc1 to Exc9 correspond to a selection in increasing excitation energy (see text). Taken from [26].

particles ($Z = 1, 2$) [21–24]. Other sortings are based on Z_{bound} (the sum of charges for fragments, $Z > 2$), as proposed by the ALADIN Collaboration [25], or on the excitation energy (NIMROD Collaboration) [26].

2.3.1 Au quasi-projectiles at relativistic energies

The ALADIN Collaboration reported the presence of bimodality for peripheral Au + Au reactions at 1 A GeV [27]. Figure 9 shows the Z_{bound} distribution (top panel) where the selected region, $Z_{bound} = 53$–55, is highlighted for which was drawn the charge asymmetry between the three largest fragments,

$$Z_1 - Z_2 - Z_3\,, \tag{3}$$

in the bottom panel. The charge asymmetry exhibits two components, the first one centered at low values (close to 0), which is associated to multifragmentation events, and the second one located at values around 40, which is more likely due to an evaporation residue of charge Z close to Z_{bound}. It is worth saying that a percolation simulation was able to reproduce this bimodality in the charge asymmetry at the transition point. In this case, this is a second-order phase transition. This point will be discussed below in the section "Pending questions".

2.3.2 A smaller system with mass ~ 40

In a very complete analysis, Ma *et al.* [26] scrutinized data collected with the NIMROD array. They were able to reconstruct, from their emitted particles and fragments, the quasi-projectiles formed in 47 A MeV Ar + Al, Ti, Ni collisions. The method used consisted in tagging the particles with the help of a three-moving-source fit (QP, QT and mid-rapidity) and then attributing to each of them, event per event, a probability to be emitted by one of these sources. Completeness of quasi-projectiles, ($Z_{QP} \geq 12$), from semi-peripheral collisions was further required; QP excitation energy was determined using the energy balance equation. The distributions of excitation energy so obtained for the three targets superimpose, showing that the QP excitation energy calculation is under control.

Plots of the charge of the second largest fragment *vs.* the largest one are shown in fig. 10. As for heavier systems, the topology evolves from residue-evaporation to multifragmentation with increasing excitation energy. An equipartition of events between two topologies is observed for $E^*/A = 5.5$ MeV, where at the same time fluctuations on the size of the largest fragment are the largest, the power law exponent for the charge distribution is minimum, and scaling laws are present. Here again, bimodality is observed at the same time as other possible indicators of a phase transition.

2.3.3 Toward a canonical event sorting?

In the previous cases the sorting for peripheral reactions uses properties of the studied source itself (here the QP) and is then probably more akin to a microcanonical than a canonical sorting. Indeed the bimodal character of the distribution is not very marked, as expected if the experimental sorting constrains strongly the excitation energy [28].

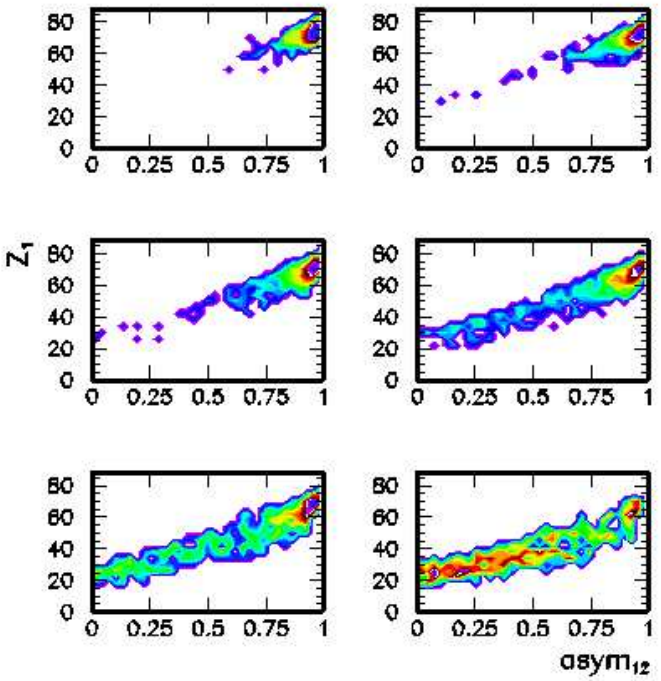

Fig. 11. Correlation between the charge of the largest fragment (Z_1) and the charge asymmetry ($asym_{12}$) between the two largest fragments for peripheral events of the Au + Au system at 35 A MeV. The panels correspond to a selection in increasing transverse energy of particles coming from the QT side from top left to bottom right. Taken from [29].

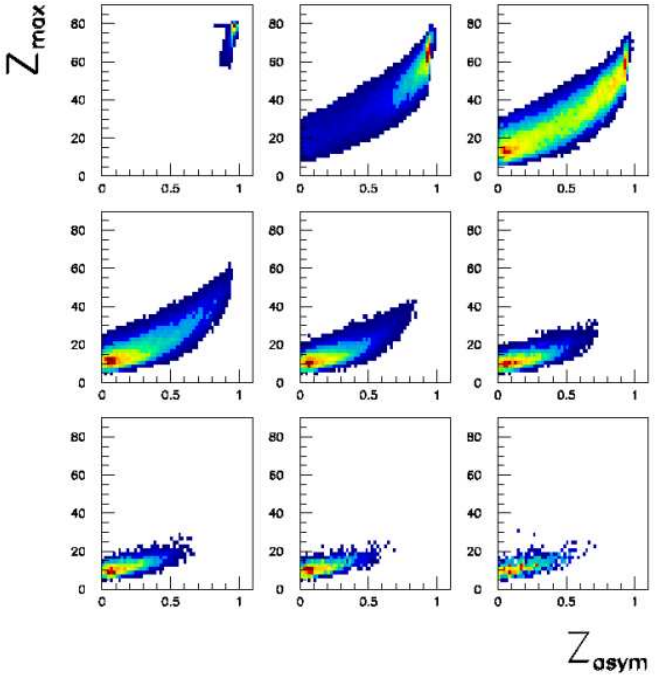

Fig. 12. Same as for fig. 11 but for Au + Au at 80 A MeV. The panels corresponds to the same cuts in QT transverse energy. Taken from [30].

To attempt a true canonical sorting one must discriminate the studied system from some heat bath. A first tentative in that aim was the study of Au quasi-projectiles through a sorting performed on the transverse energy of the particles of the Au quasi-target (as the system is symmetric, this amounts to particles emitted backward in the c.m.). This sorting is illustrated by the results presented hereafter.

2.3.4 Au-like nuclei in a "canonical" sorting

Au quasi-projectiles from Au + Au collisions at various incident energies were widely studied. Two examples are given here, at 35 A MeV —results from the MULTICS-MINIBALL Collaboration [29]— and at 80 A MeV, data from the INDRA/ALADIN Collaboration [30]. In both cases data were sorted *vs.* the transverse energy of the QT light charged particles. The charge of the largest fragment in each event is plotted in figs. 11, 12 *vs.* the charge asymmetry of the two largest fragments,

$$(Z_1 - Z_2)/(Z_1 + Z_2). \quad (4)$$

Whatever the incident energy, the picture evolves from an evaporation residue to a multifragmentation configuration, passing through a zone where the two topologies coexist, separated by a neat minimum; in this zone (last one at 35 A MeV, third one at 80 A MeV) the distributions present a bimodal behaviour. Note that the bimodal character is not very strong when one projects the bidimensional figures on either Z_{max} or on the asymmetry. This is attributed in [30] to the presence of pre-equilibrium effects, and some remaining aligned momentum which tend to shallow the minimum of a bimodal distribution.

3 Bimodality in models

Different statistical as well as dynamical models explicitly or implicitly contain a phase transition. They predict the occurrence of bimodal distributions for selected variables around some transition energy. Examples are given in this section.

3.1 SMM: Statistical Multifragmentation Model

Buyukcizmeci, Ogul and Botvina [31] analyzed SMM simulations for heavy nuclei of various sizes, with excitation energy ranging from 2 to 20 MeV/nucleon. They found that all nuclei exhibit the same caloric curve, depicted in the top panel of fig. 13, with the well-known "plateau" between 4 and 7 MeV/nucleon (note in passing that the common temperature at plateau whatever the mass of the considered nucleus is in contradiction with the experimental results analyzed in ref. [32]). In the same energy interval as that of the plateau, the fluctuations of A_{max} (not shown) and of the temperature (panel (b) of fig. 13) are maximum. The authors sorted the events following the size of the largest fragment, A_{max}. They defined two

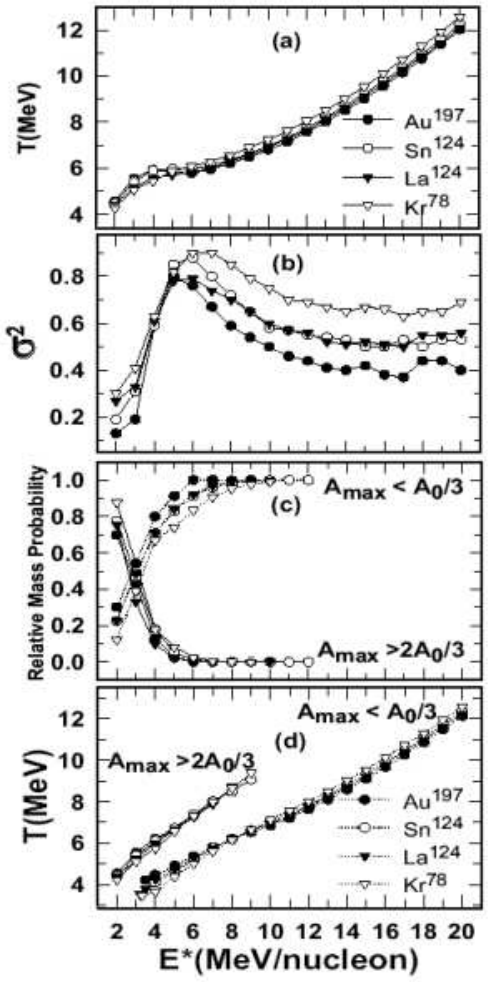

Fig. 13. Temperature average value (a) and variance (b), probability of events selected on A_{max} (c) and average temperature for these events (d) *vs.* E^* for Kr, La, Sn and Au nuclei (SMM simulations). Taken from [31].

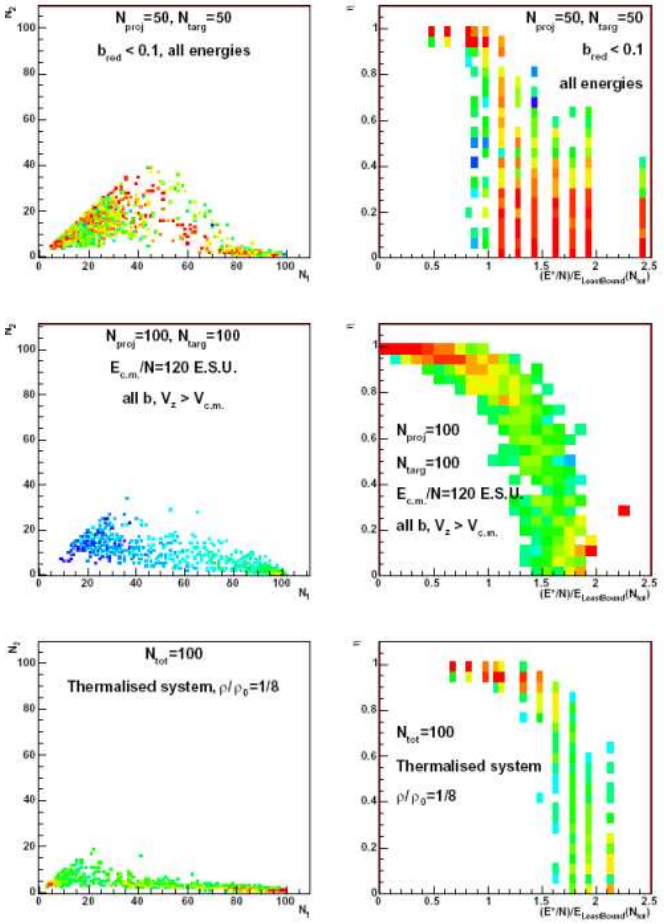

Fig. 14. Mass correlation between the two largest fragments (left) and mass asymmetry, η, as a function of the excitation energy (right), for collisions of LJ droplets. The top panel is associated to central collisions; the middle to quasi-projectiles from peripheral collisions and the bottom panel to "thermalized" systems (see text) [34].

event classes, one with $A_{max} \geq 2A_0/3$, representative of the residue-evaporation channel and the other one with $A_{max} \leq A_0/3$, characterizing multifragmentation events —A_0 being the total system size. Panel (c) of fig. 13 shows that the probability of the first group decreases rapidly in the excitation energy range 2–6 MeV/nucleon, while that of the second one increases. The temperatures T associated to each class are different, as appears on the related caloric curves: the residue-evaporation class shows a Fermi-gas behaviour (proportional to T squared), while the multifragmentation class is associated to a classical gas (linear in T). The combination of these two behaviours gives rise to the plateau zone in the total caloric curve and explains the inflexion point of this curve. One is thus dealing with a direct bimodal behaviour, with two excitation energies associated with one temperature in the transition region. This behaviour is an intrinsic feature of the phase space population in the SMM.

3.2 CMD: Classical Molecular Dynamics

Signals of phase transition were searched for in dynamical models. A simple example is a Classical Molecular Dynamics model with a Lennard-Jones potential implemented by Cussol [33]. With such a potential, analogous to the van der Waals interaction for fluids, the model includes a liquid-gas phase transition. Symmetric collisions of LJ droplets with sizes of $50 + 50$ and $100 + 100$ are analyzed. Systems were prepared in three different conditions:

- central collisions (small impact parameters),
- peripheral collisions (all impact parameters but looking at the forward zone, "quasi-projectiles"),
- "thermalized" systems (particles are placed in a box of volume $V/V_0 = 8$ and released after a time sufficient to reach thermal equilibrium).

Two variables were scrutinized, the size asymmetry between the two largest fragments, η (eq. (4)), and the mass

correlation between these same fragments [34]. The results, for systems comprising 100 droplets, are presented in fig. 14 (top: central collisions, middle: quasi-projectiles and bottom: thermalized system). Excitation energies are expressed in ESU, ratio between the excitation energy per particle and the binding energy of the least bound particle.

Bimodality —the occurrence of two fragmentation patterns in a given energy zone— is present in all situations, but at different excitation energies: 1 ESU for central collisions, 1.5 ESU for quasi-projectiles, and $\sim$ 1.8 ESU for the thermalized system. It is however worth to mention that if the thermalized system is prepared at higher densities ($\rho/\rho_0 = 1$–1.5) the transition between the fragmentation patterns also occurs but at lower excitation energy, namely < 1 ESU [34]. Cussol attributes the differences in the transition energy to the lack of complete thermalization of any source produced in nuclear collisions, whatever the impact parameter. One can conversely argue that this study proves that bimodality is a robust signature of phase transition, as it survives even if the system is not fully thermalized, although the apparent transition energy is displaced. This point will be developed later.

3.3 HIPSE: Heavy-Ion Phase Space Exploration

The Heavy-Ion Phase Space Exploration model (HIPSE) comprises a full (classical) treatment of the entrance channel (nucleus-nucleus potential, NN collisions). It is followed by a random sampling of nucleons in the participant zone from Thomas-Fermi distributions of the two colliding nuclei to form fragments in the dense zone [35]. Excitation energy is shared among all products, taking into account the total energy constraint. Finally a statistical de-excitation (SIMON code [36]) of the fragments, including QP and QT —if they are still present— is performed.

Simulations were done for all impact parameters, to mimick a real $50\,A$ MeV Xe + Sn experiment, then the same analysis as in [30] was performed by Lopez *et al.* [37]; a bimodal structure was observed in the correlation between Z_{max} and the charge asymmetry of the two largest fragments (eq. (4)). In a model however one can go further and track the origin of the bimodal behaviour: is it due to the entrance channel (dynamical effect) or to the de-excitation step? The first hypothesis was ruled out, as no discontinuity was found in the evolution of the size of the hot largest fragment with the impact parameter: the bimodality was clearly attributed to the statistical de-excitation of the QP. A deeper analysis of the de-excitation stage was then achieved through the simulated statistical de-excitation of xenon nuclei of different excitation energies and spins with the SIMON code [36]. This is depicted in fig. 15, where the distributions of the asymmetry variable (eq. (4)) are plotted for several initial conditions. Increasing the excitation energy does decrease the average charge asymmetry, but never down to the small values observed in the data. Conversely, if more spin is given to the nucleus, the asymmetry variable displays a sharp transition around 60–70$\hbar$, which corresponds indeed to the angular momentum for which the symmetric fission barrier vanishes.

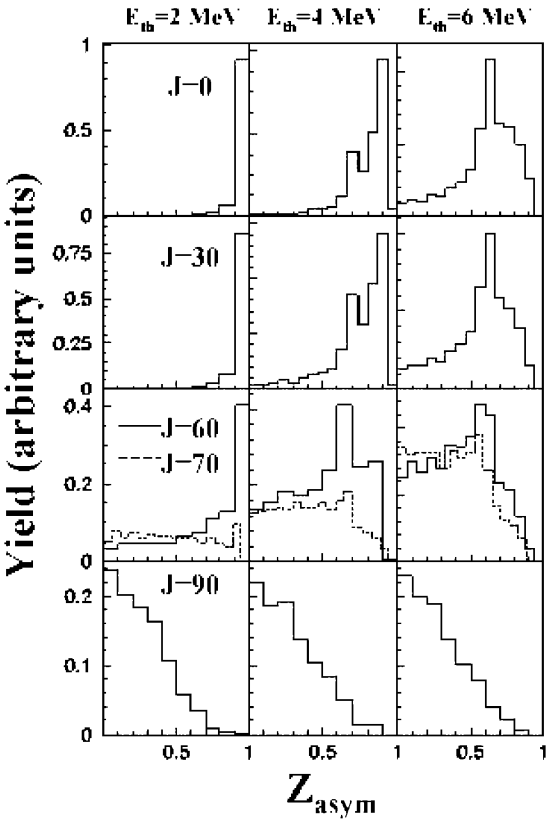

Fig. 15. Charge asymmetry distributions resulting from the de-excitation of hot Sn nuclei with different initial excitation energies (columns) and spin (rows), with the SIMON code. Taken from [37].

The authors of [37] conclude that, in the HIPSE model, the observed bimodality found its origin in the spin rather than in the excitation energy transferred to the QP, being still a phase transition but not of the liquid-gas type. It is worth mentioning that using the SMM model for the de-excitation stage, the authors also observe bimodality in the size of the largest fragment. This is not surprising in view of the abovementioned study with the SMM. However, this raises the important issue —still under debate— of the order parameters (and then the type of the phase transition) which govern the bimodality. This point will be discussed below in the section "Perspectives".

4 Pending questions

As seen in the previous sections, bimodality is a very common feature in nuclear collisions at intermediate energies. It is present in central as well as in peripheral collisions. It takes place for a large range of masses, $A = 40$–200. It was however mentioned in the course of the text that it is experimentally difficult to isolate a source, because of dynamical effects leading to a mixture of pre-equilibrium

Table 1. World-wide experimental results on bimodality recorded in July 2005.

Results from	Reaction centrality	Source size	Bimodal variable
INDRA	Central	~ 200	$Z_1 - Z_2$ (eqs. (1), (4))
INDRA	Central	~ 200	$Z_{liq} - Z_{gas}$ (eq. (2))
INDRA	Central	~ 100	Z_{max}
INDRA	Peripheral	160–180	$Z_1 - Z_2$ (eq. (4))
MULTICS/ MINIBALL	Peripheral	~ 180	$Z_1 - Z_2$ (eq. (4))
ALADIN	Peripheral	~ 130	$Z_1 - Z_2 - Z_3$ (eq. (3))
NIMROD	Peripheral	24–40	$Z_{liq} - Z_{gas}$

products and of QP/QT de-excitation particles. Even if a source can be properly defined, one has to verify its degree of thermalization. Indeed radial flow was found, particularly in central collisions, and transparency effects were also evidenced [38]. It seems however from both experimental [30] and theoretical [37] studies that bimodality is not mainly driven by dynamical effects. Ambiguities remain in the type of phase transition observed, and consequently on the definition of a true order parameter. Some of these questions were addressed recently and are presented in the following.

Table 1 gathers all experimental results on bimodality found so far. A glance at the table indicates that bimodality was essentially found in charge asymmetry variables comprising the two or three largest fragments of each event. Such variables can in some sense be related to the density difference between a dense (liquid) and a dilute (gas) phase; in some models, for instance the Fisher droplet model, the largest fragment is assimilated to the liquid while all the other form the gas.

4.1 Are Z_{max}, A_{max}, or the asymmetry order parameters?

Simulations were performed in different frameworks to test whether the observables Z_{max}, A_{max}, or the asymmetry, reliably sign a phase transition. Let us recall that a bimodality of an order parameter signs the occurrence of a first-order phase transition in a finite system. Figure 16 shows the outcomes of three simulations in the transition region —when it exists; there is no phase transition in the random partitions calculation, while percolation has a second-order transition and lattice gas a first-order one [39]. The distributions of the largest fragment A_{max} evidence that A_{max} only presents a bimodal distribution for the canonical lattice-gas calculation. This means that A_{max} is indeed an order parameter of the first-order phase transition of the lattice gas. The distribution presents a wide plateau, as expected, in the case of a continuous transition (percolation). By contrast, the mass asymmetry, A_{asy}, defined in a similar way as the charge asymmetry (eq. (4)), also displays a bimodality (although with a less marked minimum) for simulations which have a

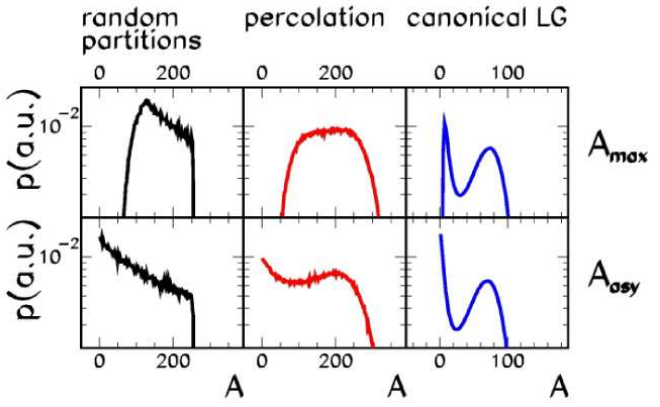

Fig. 16. Largest fragment A_{max} (top) and mass asymmetry A_{asy} (bottom) distributions for three simulations. Left: random partitions (no phase transition), middle: percolation (2nd-order phase transition) and right: canonical lattice gas (1st-order phase transition). Taken from [39].

2nd-order phase transition (percolation, middle column). The conclusion of this study is that both A_{max} and A_{asy} clearly signal a phase transition —note that none of them presents bimodality in a model without phase transition— but A_{max} is the only unambiguous signature of the order of the transition.

4.2 Order parameters of the liquid-gas phase transition

If nuclei undergo a liquid-gas–type phase transition, then the order parameters are known: energy, volume. In some of the experimental studies cited above, the authors try to push the analysis beyond the single observation of bimodality on the asymmetry variable. As a first attempt, in central collisions between Ni and Au at 52 A MeV [10], the excitation energies (experimentally deduced from the energy balance equation) associated to the two fragmentation patterns were found slightly different (by 1 A MeV) [40]. This bimodality of the excitation energy is an indication in favour of the liquid-gas type of the phase transition observed.

Studies of Au quasi-projectiles were deepened by the authors of ref. [30]: a test of the reliability of the canonical picture was accomplished by estimating the apparent temperatures of the two types of events, from the slope of the emitted proton spectra for residue-like events, and from double isotope ratios in the multifragmentation regime. As seen in fig. 17 both temperatures are close enough in the region where bimodality is present (Etrans = 0.8–1.2 A MeV), while the excitation energies, calculated with the energy balance equation, are different. This is expected if bimodality has a thermal origin and validates the sorting as close to a canonical one.

4.3 Does bimodality survive out-of-equilibrium effects?

The influence of non-equilibrium effects on signals of phase transition was studied in [41] in the case of incompletely

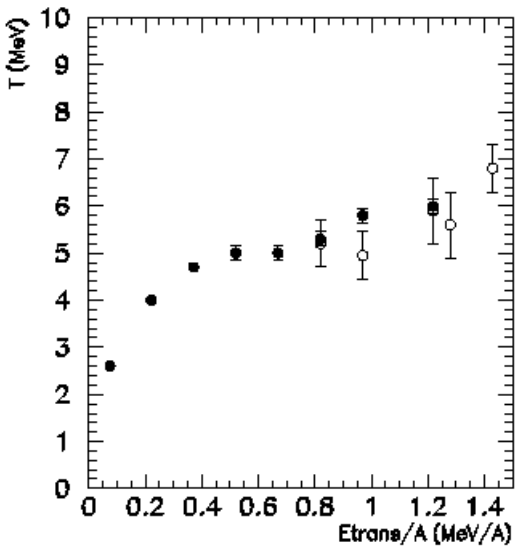

Fig. 17. Apparent temperatures of Au quasi-projectiles as a function of the normalized transverse energy for residue (filled symbols) and multifragmentation events (open symbols). Taken from [30].

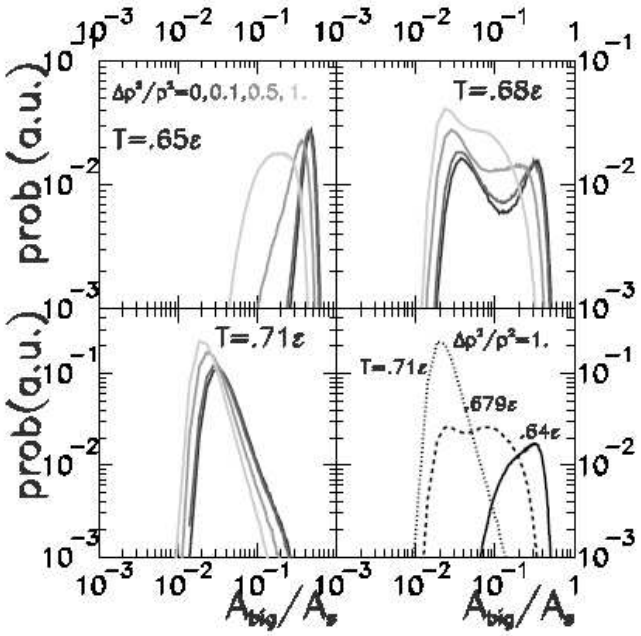

Fig. 18. Canonical lattice-gas simulations for different temperatures T around the critical one $T_c = 0.68\varepsilon$ for the distributions of the largest fragment. Simulations are performed by adding an extra radial-flow energy $\Delta p^2/p^2$ between 0 and 1. Taken from [2].

relaxed incoming momentum (transparency) and of self-similar radial flow. Both effects were indeed recognized in experimental data. Figure 18 displays results of (canonical) lattice-gas simulations with different radial-flow energies; $\Delta p^2/p^2$ is equivalent to the ratio $\varepsilon_{flow}/\varepsilon_{th}$ and is varied from 0 to 1. At the transition temperature, $T = 0.68\varepsilon$, a bimodality of A_{max} is clearly seen in the absence of flow, and is still visible even when the flow energy is as important as the thermal energy (top right panel). The authors state thus that radial flow does disturb the signal, partially filling the gap between the two components, but does not destroy it as long as the flow does not dominate the global energetics. Similar conclusions were drawn in this paper in the presence of longitudinal flow (transparency effects).

These two examples illustrate the robustness of bimodality *vs.* external (and realistic) constraints due to the dynamics of the collision; similar conclusions can also be derived from CMD simulations (see above).

In experimental data on Au quasi-projectiles [30], refined treatments aiming at better isolating quasi-projectiles from the mid-rapidity contribution and keeping only events where this contribution was smaller were tempted. In all cases the bimodal picture comes out better, although it occurs for a lower value of the sorting variable (smaller dissipation), for a given incident energy. This is again an evidence of the robustness of bimodality against non-equilibrium effects.

5 Perspectives

Bimodality is a very promising signature of first-order phase transition because of its simplicity and robustness against dynamical constraints. It was shown in this contribution that the signal is quite common for the decay of hot nuclei and can be observed in rather different experimental conditions (central/peripheral collisions, small/large source sizes).

Nevertheless, some open questions need to be answered in order to firmly assess the validity of this signal. Several strategies can be envisaged in order to progress in this direction:

- cross the observation of the bimodality signal with that of all the other proposed signals for the phase transition such as critical exponents, scalings (Delta-scaling, Fisher scaling, Zipf law), negative heat capacities, or space-time correlations (emission times and correlation functions). Obviously, when possible, all signals should be studied on the same sample of events to minimise biases due to sorting. Such cross controls were started by the INDRA [42] and NIMROD [26] Collaborations. One must solve however the problem of the non-equivalence of statistical ensembles in some cases.
- Test the effect of sorting. Indeed different ways of sorting were proposed (impact parameter selectors, compact shape events, source selection). The robustness of any signal will be established if its observation is not drastically dependent on the chosen sorting for a given centrality, for instance.
- Compare the results of different entrance channels for nuclear collisions; by using asymmetrical reactions such as light ions impinging on heavy targets, or nucleon/pion-nucleus reactions, one may hope to disentangle the different effects which could possibly govern bimodality. By using these very different entrance

channels reactions, the pre-equilibrium/neck contributions can be evaluated and even subtracted. Moreover, the effects of large collective motions such as radial flow (for central collisions) or spin (angular-momentum transfer in semi-peripheral reactions) can also be measured. This will possibly help to answer the fundamental question of the type of phase transition which is experienced by hot nuclei.

We thank all the nuclear physicists around the world who send us their results —published or not.

References

1. T.L. Hill, *Thermodynamics of Small Systems* (Benjamin, New York, 1963).
2. Ph. Chomaz, F. Gulminelli, V. Duflot, Phys. Rev. E **64**, 046114 (2001).
3. K.C. Lee, Phys. Rev. E **53**, 6558 (1996).
4. K. Binder, D.P. Landau, Phys. Rev. B **30**, 1477 (1984).
5. Ph. Chomaz, F. Gulminelli, Physica A **330**, 451 (2003).
6. C.N. Yang, T.D. Lee, Phys. Rev. **87**, 404 (1952).
7. Ph. Chomaz, M. Colonna, J. Randrup, Phys. Rep. **389**, 263 (2004).
8. D.H.E. Gross, *Lecture Notes in Physics*, Vol. **602** (Springer-Verlag, 2002) p. 23.
9. M.S. Challa, J.H. Hetherington, Phys. Rev. Lett. **60**, 77 (1988).
10. INDRA Collaboration (N. Bellaize *et al.*), Nucl. Phys. A **709**, 367 (2002).
11. B. Borderie, J. Phys. G: Nucl. Part. Phys. **28**, R217 (2002).
12. Ph. Chomaz, G.F. Burgio, J. Randrup, Phys. Lett. B **254**, 340 (1991); A. Guarnera, Ph. Chomaz, M. Colonna, J. Randrup, Phys. Lett. B **403**, 191 (1997).
13. INDRA Collaboration (J.D. Frankland *et al.*), Nucl. Phys. A **689**, 940 (2001).
14. INDRA Collaboration (G. Tăbăcaru *et al.*), Eur. Phys. J. A **18**, 103 (2003).
15. INDRA Collaboration (G. Tăbăcaru *et al.*), Nucl. Phys. A **764**, 371 (2006).
16. INDRA Collaboration (P. Lautesse *et al.*), Phys. Rev. C **71**, 034602 (2005).
17. P. Lautesse, Habilitation à diriger des recherches, Université Claude Bernard Lyon I (2006); R. Moustabchir, thèse de doctorat, Québec/Lyon (2005), `http://tel.ccsd.cnrs.fr/tel-00008654`.
18. INDRA Collaboration (N. Marie *et al.*), Phys. Lett. B **391**, 15 (1997).
19. N. Le Neindre, thèse de doctorat, Caen (1999), `http://tel.ccsd.cnrs.fr/tel-00003741`.
20. INDRA Collaboration (B. Borderie *et al.*), Nucl. Phys. A **734**, 495 (2004).
21. W.J. Llope *et al.*, Phys. Rev. C **51**, 1325 (1995).
22. J. Péter *et al.*, Nucl. Phys. A **593**, 95 (1995).
23. INDRA Collaboration (J. Lukasik *et al.*), Phys. Rev. C **55**, 1906 (1997).
24. INDRA Collaboration (J.D. Frankland *et al.*), Nucl. Phys. A **689**, 905 (2001).
25. A. Schüttauf *et al.*, Nucl. Phys. A **607**, 457 (1996).
26. NIMROD Collaboration (Y.G. Ma *et al.*), nucl-ex/0410018.
27. ALADIN Collaboration (W. Trautmann *et al.*), private communication (2005).
28. F. Gulminelli, Ph. Chomaz, Phys. Rev. C **71**, 054607 (2005).
29. MULTICS-MINIBALL Collaboration (M. d'Agostino *et al.*), private communication (2004).
30. INDRA Collaboration (M. Pichon *et al.*), Nucl. Phys. A **749**, 93c (2004); nucl-ex/0602003; M. Pichon, thèse de doctorat, Caen (2004), `http://tel.ccsd.cnrs.fr/tel-00007451`.
31. N. Buyukcizmeci, R. Ogul, A.S. Botvina, Eur. Phys. J. A **25**, 57 (2005).
32. J.B. Natowitz *et al.*, Phys. Rev. C **65**, 034618 (2002).
33. D. Cussol, Phys. Rev. C **65**, 054614 (2002).
34. D. Cussol, private communication (2005).
35. D. Lacroix, A. Van Lauwe, D. Durand, Phys. Rev. C **69**, 054604 (2004).
36. D. Durand, Nucl. Phys. A **541**, 266 (1992).
37. O. Lopez, D. Lacroix, E. Vient, Phys. Rev. Lett. **95**, 242701 (2005).
38. W. Reisdorf *et al.*, Phys. Rev. Lett. **92**, 232301 (2004); INDRA Collaboration (C. Escaño-Rodriguez *et al.*), nucl-ex/0503007.
39. F. Gulminelli, private communication (2005).
40. O. Lopez, unpublished results.
41. F. Gulminelli, P. Chomaz, Nucl. Phys. A **734**, 581 (2004).
42. INDRA Collaboration (M.F. Rivet *et al.*), Nucl. Phys. A **749**, 73 (2005).